ELSEVIER

Cold Regions Science and Technology 26 (1997) 113–135

cold regions science and technology

Modelling the dynamics and thermodynamics of icebergs

Grant R. Bigg [a,*], Martin R. Wadley [a], David P. Stevens [b], John A. Johnson [b]

[a] *School of Environmental Sciences, University of East Anglia, Norwich NR4 7TJ, UK*
[b] *School of Mathematics, University of East Anglia, Norwich NR4 7TJ, UK*

Received 13 November 1996; accepted 23 April 1997

Abstract

Icebergs are a significant hazard for polar shipping, and, geophysically, are significant components of the mass balance of continental ice sheets while providing major freshwater inputs to the polar oceans. Some modelling of iceberg trajectories has been undertaken in the past, principally in the Labrador Sea, but here we present a hemispheric-wide attempt to model iceberg motion in the Arctic and North Atlantic Oceans. We show that the basic force balance in iceberg motion is between water drag and water advection, but with the pure geostrophic balance being only a minor component of the latter. Iceberg density maps essentially demonstrate the effect of the major boundary currents but we show that the time and size of calving from individual tidewater glaciers are important variables in determining the ultimate fate of bergs. The biggest bergs never leave the Arctic Ocean. All modelled icebergs have melted after about 5 years from their release date, although most melt over the first year. During their lifetime most, but not all bergs, overturn several times. Our model shows good agreement with the limited observational data. We therefore suggest that icebergs, both modelled and observed, may be exploited as previously little-used geophysical tracers. © 1997 Elsevier Science B.V.

Keywords: iceberg; numerical modelling; trajectories; Arctic; North Atlantic

1. Introduction

It is commonly held that icebergs drift relative to the ocean current at 2% of the wind speed (Smith and Donaldson, 1987). This statement suggests that the ocean current determines the direction of an iceberg's drift, but that the wind moderates its speed. We will see in Section 4.1 that this is indeed true but iceberg motion is potentially affected by more processes than just water advection and air form drag. These can include water drag, ice drag and wave drag. The process of advection by the ocean current is also more complex than at first appears (Bigg et al., 1996). Icebergs additionally change shape and mass during their lifetimes. Much information has been gathered about iceberg locations in the Labrador Sea since the inception of the International Ice Patrol (Strübing, 1974) following the 'Titanic' disaster in 1912 (e.g. Gustajtis and Buckley, 1978; Robe et al., 1980; Marko et al., 1982; Venkatesh and El-Tahan, 1988; Marko et al., 1994). Other areas are less well surveyed, although the Barents Sea (Abramov, 1992) and Antarctic waters (Weeks and Mellor, 1978; Morgan and Budd, 1978) have significant data sets. However, relatively little is known about the details of individual iceberg trajectories over long distances, apart from general conceptions of large-scale movements (e.g. Marko et al., 1994).

* Corresponding author. Fax: 44-1603-507719; e-mail: g.bigg@uea.ac.uk

PII S0165-232X(97)00012-8

Modelling efforts in the past have concentrated on short-term prediction of iceberg movement, validated by at most a few days tracking of bergs (Smith and Banke, 1983; Smith and Donaldson, 1987; Isaacson and McTaggart, 1990; Smith, 1993). Some of these have been of a statistical nature, rather than relying on physics to generate the iceberg tracks (Garrett, 1985). Løset (1993) attempted to hindcast the track of a grounded berg prior to its grounding for a few hundred kilometres.

A major drawback in understanding and modelling iceberg motion has been the paucity of ocean current data to provide the basic driving mechanism. In this paper, we circumvent this difficulty by using the current field of a three-dimensional ocean general circulation model, and its forcing wind and surface air temperature fields, to drive icebergs released from the major tidewater glaciers throughout the North Atlantic and Arctic Oceans. In a companion paper (Bigg et al., 1996) we have shown that our iceberg model, similar to that of Smith (1993), but also incorporating thermodynamics, reproduces the general iceberg limits encountered in the North Atlantic. Here, we concentrate on describing the model details (Sections 2 and 3), the variation in the relative forcing terms over the northern seas (Section 4.1), and the life history of icebergs (Sections 4.2, 4.3, 4.4 and 4.5). A finer resolution model of the Greenland area is used to check the degree to which the trajectories generated by the coarser model are a result of the resolution of the oceanic current features (Section 4.6). We then discuss how our modelled trajectories compare with observations (Section 5) and speculate on how iceberg–ocean models could be used for both glaciological and oceanographical purposes beyond simply modelling iceberg trajectories (Section 6).

2. Iceberg calving and size distribution

In order to realistically seed the ocean model with icebergs we needed to decide on (i) appropriate calving sites, (ii) approximate calving rates, and (iii) a spectrum of typical sizes appropriate to a given calving rate. The latter issue was the simplest to resolve and has implications for the other two points, as will be seen below.

Several authors have shown that icebergs of both Arctic and Antarctic origin have a log-normal distribution of length, with a sharp decline in numbers above 1 km, but relatively large numbers of bergs under 500 m in length (Weeks and Mellor, 1978; Morgan and Budd, 1978; Dowdeswell et al., 1992). We therefore allowed up to ten different initial sizes (Table 1) of bergs for each source point, with the number of size classes used depending on the calving rate. For later calculation of iceberg density (Section 4.2) the fraction of bergs assumed to be in each size class was taken from Antarctic data of Morgan and Budd (1978), although this may overestimate Northern Hemisphere sizes if the Scoresby Sund distribution of Dowdeswell et al. (1992) is representative of bergs of fjord origin that reach the open ocean.

We used a width : length ratio of 1 : 1.5, which is similar to the mean figures of 1 : 1.62 and 1 : 1.6 found by Dowdeswell et al. (1992) and Morgan and Budd (1978), respectively; nonetheless this ratio is a very variable number (Weeks and Mellor, 1978). The thickness of an iceberg depends very much on

Table 1
Initial size classes for iceberg model

Size class	Fraction (%)	Length (m)	Width (m)	Draught (m)	Freeboard (m)	Mass (10^9 kg)
1	15	100	67	67	13.4	0.491
2	15	200	133	133	26.5	3.88
3	20	300	200	200	40.0	13.1
4	15	400	267	267	53.0	31.2
5	8	500	333	300	60.0	54.7
6	7	600	400	300	60.0	78.8
7	5	750	500	300	60.0	123.0
8	5	900	600	300	60.0	177.0
9	5	1200	800	300	60.0	315.0
10	5	1500	1000	300	60.0	492.0

Table 2
Initial iceberg size distribution and calving rate

Calving rate CR (km^3 yr^{-1})	Size classes released
$CR \leq 0.5$	1–5
$0.5 < CR \leq 1.0$	1–6
$1.0 < CR \leq 2.0$	1–7
$2.0 < CR \leq 5.0$	1–8
$CR > 5.0$	1–10

the glacier from which it calved. Dowdeswell et al. (1992) found a weak correlation between length and keel depth, but Orheim (1987) suggests that a rough equality between width and depth exists, at least for bergs up to 200–250 m in width, although both Dowdeswell et al. (1992) and Orheim (1987) suggest that there is a similar maximum thickness for even bigger bergs. Our compromise was to allow the draught to equal the width (the shorter horizontal dimension) up to size class 4, but to then cap the draught at 300 m for all larger bergs.

The remaining ratio was that of the freeboard to draught. The density of pure ice (used to calculate the berg mass) would suggest that 13% of the berg should be out of the seawater. However, even the

Table 3
Source locations for icebergs and regional calving rate

Seed location	Calving rate of largest glacier (km^3 yr^{-1})	Total flux from region (km^3 yr^{-1})	Maximum size class released	Comments
83.0°N, 60.0°W	0.8	0.8	6	North Greenland
84.0°N, 50.0°W	2.0	2.0	8	id.
83.5°N, 20.0°W	0.8	0.8	6	id.
75.0°N, 65.0°W	2.9	4.9	8	West Greenland
71.5°N, 60.0°W	> 10	> 10	10	id.
69.2°N, 59.0°W	35	35	10	Jacobshavn
64.0°N, 57.0°W	2.8	2.8	8	id.
61.0°N, 53.0°W	2.1	2.1	8	id.
59.0°N, 49.0°W	1.0	1.0	7	id.
58.5°N, 43.5°W	0.4	0.4	5	East Greenland
60.8°N, 42.0°W	0.4	0.9	5	id.
63.0°N, 42.0°W	2.3	5.0	8	id.
64.5°N, 38.0°W	3.0	6.0	8	id.
68.0°N, 31.0°W	3.0	3.0	8	id.
70.3°N, 21.0°W	3.0	3.0	8	id.
73.0°N, 21.0°W	3.0	3.0	8	id.
75.2°N, 18.7°W	1.2	2.0	7	id.
79.0°N, 17.0°W	3.0	3.0	8	id.
81.0°N, 10.0°W	2.3	2.3	8	id.
83.0°N, 12.0°W	3.0	3.0	8	id.
83.5°N, 92.5°W	2.1	3.4	8	N. Ellesmere Is.
83.5°N, 84.0°W	12.3	15.1	10	id.
83.5°N, 72.0°W	5.4	5.4	10	id.
76.0°N, 73.0°W	16.6	48.3	10	Nares Strait
74.0°N, 78.0°W	3.3	14.0	8	Devon and Bylot Is.
68.5°N, 63.0°W	0.1	0.1	5	S. Baffin Is.
79.5°N, 33.0°E	2.0	3.2	8	Nordaustlandet and Kuitaya
78.5°N, 5.0°E	1.8	2.2	7	W. Spitzbergen
77.5°N, 22.0°E	0.9	0.9	6	Edgeøya
81.0°N, 50.0°E	> 10	> 10	10	W. Franz Josef Land
81.0°N, 63.0°E	6.1	7.3	10	E. Franz Josef Land
74.4°N, 65.0°E	1.0	1.0	7	Novaya Zemlya
77.5°N, 63.0°E	1.0	1.0	7	id.
81.0°N, 80.0°E	1.2	1.2	7	Severnaya Zemlya
80.2°N, 85.0°E	5.4	6.8	10	id.
80.2°N, 109°E	6.0	6.9	10	id.

relatively tabular bergs of the Southern Ocean can have 18% of their thickness above water (due to wave terracing, Weeks and Mellor, 1978). Thus, as a compromise between our assumption of the bergs as rectangular parallelepipeds and taking account of their real windage, we have assumed a ratio of draught to freeboard of 5 : 1 (16.7%). This is consistent with the estimate of Harvey (1976) for Arctic bergs, and gives a maximum freeboard consistent with observations quoted in Morgan and Budd (1978).

Remarkably few calving fluxes appear in the literature for individual glaciers or fjords. These included the fjords of northern Greenland (3.4 km^3 yr^{-1}; Higgins, 1990); Kangerdlugssuaq and Nansen fjords (15 and 2 km^3 yr^{-1}, respectively; Andrews et al., 1994) and Scoresby Sund (18 km^3 yr^{-1}; Dowdeswell et al., 1992) in eastern Greenland; Jakobshavn (35 km^3 yr^{-1}; Warren, 1992) in western Greenland; and Novaya Zemlya and Svalbard (2 and 1 km^3 yr^{-1}, respectively; Koryakin, 1986). The latter two were derived from measurements of long-term change in ice cover rather than more direct measurements. As we are not trying to model every iceberg's trajectory, but only the paths of those of representative sizes, we merely require rough estimates of calving rates so as to decide on the appropriate size classes with which to initialise given source points. The allocation of size classes for given regional calving rates is shown in Table 2. It is a function of the cumulative volume of the size classes in Table 1, for example the cumulative volume for one berg of each size from 1 to 5 inclusive is 0.11 km^3 while for all classes it is 1.41 km^3.

To identify the initial positions for our sets of icebergs, we examined bathymetric, glacial and geological maps of the Arctic Ocean, Greenland coast and Canadian Arctic. The locations of tidewater glaciers, floating iceshelves and icecaps were identified. The calving rate for individual glaciers can then be estimated from multiplying the product of the map-derived near-shore ice height and glacier width by the calving velocity, v_c, the latter being derived from the empirical but robust formula of Pelto and Warren (1991):

$$v_c = 70 + 8.33h_w \quad (1)$$

where h_w is the water depth in metres and v_c is in m yr^{-1}. A number of calving sites are close together. Taking the 1° horizontal resolution of the driving ocean model into account, it is sensible to combine close sites. This leads to a total of 36 calving sites (see Fig. 3). These are listed in Table 3, with our estimate of the largest individual glacier's annual calving rate in each of the 36 regions and the total regional iceberg flux. The latter broadly agree with existing data where this was quoted above, although the Scoresby Sund estimated rate is rather lower.

3. Basic equations and numerical model

3.1. Dynamics

Our basic equation describing the horizontal motion of an iceberg of mass M at position X, moving with horizontal velocity $\boldsymbol{V}_i$, is:

$$M\frac{d\boldsymbol{V}_i}{dt} = -Mf\boldsymbol{k}\boldsymbol{x}\boldsymbol{V}_i + \boldsymbol{F}_a + \boldsymbol{F}_w + \boldsymbol{F}_r + \boldsymbol{F}_s + \boldsymbol{F}_p \quad (2)$$

where f is the Coriolis parameter, $\boldsymbol{F}_a$ is the air form drag, $\boldsymbol{F}_w$ is the water drag, $\boldsymbol{F}_r$ is the wave radiation force, $\boldsymbol{F}_s$ is the sea-ice drag (where applicable) and $\boldsymbol{F}_p$ is the horizontal pressure gradient force exerted by the water on the volume that the iceberg displaces. As in Smith (1993), the general drag relationship is given by:

$$\boldsymbol{F}_x = \frac{1}{2}\rho_x C_x A_x |\boldsymbol{V}_x - \boldsymbol{V}_i|(\boldsymbol{V}_x - \boldsymbol{V}_i) \quad (3)$$

where the subscript x refers to air (a), water (w) or sea-ice (s), respectively, ρ_x is the appropriate density, C_x is the drag coefficient ($C_a = 1.3$, $C_w = 0.9$, from Chirivella and Miller (1978) and Smith (1993) and $C_s = C_w$), and A_x is the appropriate cross-sectional area of the berg where it is affected by the stressing medium in a vertical plane normal to the stressing flow, which has velocity $\boldsymbol{V}_x$. The sea-ice is assumed to move with the water. The wave radiation force is:

$$\boldsymbol{F}_r = \frac{1}{4}\rho_w g a^2 L \frac{\boldsymbol{V}_a}{|\boldsymbol{V}_a|} \quad (4)$$

where L is the length of the berg normal to incident waves of amplitude a which are assumed to have the same direction as $\boldsymbol{V}_a$ (Smith, 1993) and g is the gravitational acceleration. The wave amplitude was

estimated from a quadratic fit of wave height, h (in m), to wind speed, $|\boldsymbol{V}_a|$ (in m s^{-1}), from data in the marine Beaufort scale (Meteorological Office, 1969):

$$h = 2a = 0.02025|\boldsymbol{V}_a|^2 \quad (5)$$

The pressure gradient force, $\boldsymbol{F}_p = -M(\nabla P)/\rho_w$, is the basic force causing motion in the water around the iceberg. This can be found by re-arranging the following equation of motion for $\boldsymbol{V}_w$, which in terms of forces per unit mass is:

$$\frac{d\boldsymbol{V}_w}{dt} + \boldsymbol{f}\boldsymbol{k}\boldsymbol{x}\boldsymbol{V}_w = -\frac{1}{\rho}\nabla P + \frac{1}{\rho}\frac{\partial \tau}{\partial z} \quad (6)$$

where P is the horizontal pressure field, τ is the surface wind stress and z is the vertical coordinate. In practice the surface wind stress term reduces to the product of the inverse Ekman depth, E_k^{-1}, and the surface wind stress, τ_s ($= 1.5 \times 10^{-3}\ \rho_a|\boldsymbol{V}_a|\boldsymbol{V}_a$, Gill (1982)), where E_k is taken to be the draught of the iceberg, or 90 m, whichever is shallower.

It has been common (e.g. Smith and Banke, 1983; Løset, 1993) to assume that the ocean is in steady, geostrophic equilibrium and that the pressure force per unit mass on an iceberg is then just $\boldsymbol{f}\boldsymbol{k}\boldsymbol{x}\boldsymbol{V}_w$. Bigg et al. (1996) have shown, however, that the dominant term in a rearrangement of Eq. (6) for $\boldsymbol{F}_p/M$ is the material derivative $d\boldsymbol{V}_w/dt$, and that this component of $\boldsymbol{F}_p/M$ is the principal factor needed to reproduce realistic iceberg distributions. Later (Section 4.1) we will examine the spatial variability in this term, but its general importance stems not only from the strong seasonal variability in both atmospheric and oceanic flows in the polar seas, but also from the non-linearities induced by the strong, horizontally sheared flows in the Labrador and Greenland Seas.

Each berg is assumed to be travelling with its long axis parallel to the surrounding water flow, but also to be oriented so that $\boldsymbol{V}_a$ is 45° to the left of the berg (in the Northern Hemisphere). These two conditions should be mutually compatible according to Ekman theory, but in practice will not always be so. However, any errors due to these assumptions should be of the same magnitude as those inherent in the drag approximation (Eq. (3)). We have also neglected the added mass due to entrained melt-water carried along with the berg, as suggested by Smith (1993).

A further dynamic constraint is imposed by the tendency of icebergs to preferentially erode laterally rather than vertically. We thus allow a berg to roll onto its side instantaneously once some stability constraint has been reached. The constraint used to determine whether a berg is stable is the Weeks–Mellor criterion (Weeks and Mellor, 1978):

$$\frac{L_a}{T} > \sqrt{0.92 + \frac{58.32}{T}} \quad (7)$$

where T is the total vertical extent of the berg (in m) and L_a (in m) is its horizontal long axis. The sensitivity of iceberg trajectories to this roll over criterion is discussed in Section 4.5.

3.2. Thermodynamics

The melting of an iceberg constantly changes its mass and shape, and thus must be modelled in any long-term simulation of trajectories. Løset (1993) modelled the melting of an individual iceberg in detail using finite-element techniques, but here a more empirical approach is needed because of the large number of bergs being studied. The melting/erosional processes that have been included are 'basal' convection or turbulent heat transfer, buoyant convection, wave erosion, solar and sensible heating, and sublimation.

The relative motion of the water past the iceberg generates turbulence that acts to carry heat to the berg. This 'basal' turbulent heat transfer also occurs on the sides of the berg past which the water flows. Weeks and Campbell (1973) used the general theory of Eckart and Drake (1959) for heat transfer past a flat plate to derive a 'basal' turbulent melting rate, M_b, in m day^{-1}, applicable to icebergs:

$$M_b = 0.58|\boldsymbol{V}_w - \boldsymbol{V}_i|^{0.8}\frac{T_w - T_i}{L_a^{0.2}} \quad (8)$$

where T_i is the surface temperature of the ice (in °C) and T_w is the water temperature (in °C). The former is taken to be −4°C, the equilibrium ice skin temperature in the high resolution melting study of Løset (1993), while the latter is taken to be the sea surface temperature. The latter assumption will tend to artificially accentuate melting as the iceberg moves into warmer waters because the iceberg is then surrounded by a significant train of cold meltwater.

Buoyant convection occurs on the sides of the berg due to the temperature contrast between the ice

and water. El-Tahan et al. (1987) developed an empirical relationship for the melting rate for the overall iceberg length, M_v, in m day^{-1}, due to heat transferred in this fashion, namely:

$$M_v = 7.62 \times 10^{-3} T_w + 1.29 \times 10^{-3} T_w^2 \quad (9)$$

Another, in fact the major, erosional loss is due to wave erosion. This occurs both above and below the mean water line. El-Tahan et al. (1987) observed that a sea state of 1–2 (i.e. ripples to small wavelets, with no wave breaking) caused 0.5–1 m of erosion per day; we have extrapolated this observation in the spirit of the F_r relationship (Eq. (4) to an erosional loss, M_e, in m day^{-1}, of:

$$M_e = 0.5 S_s \quad (10)$$

where S_s is the sea state, calculated as a function of wind speed according to the marine Beaufort scale (Meteorological Office, 1969). Note that wave erosion has sometimes been thought to depend on water temperature. The latter must be important, because, for T_s above 0°C, the warmer water acts to weaken the outer fabric of the iceberg. However, we use Eq. (10) rather than invent a function of sea state and temperature as the former must be the physical mechanism responsible for erosion. Despite the crudity of Eq. (10), our results suggest that this approximation is not outrageously poor, and may underestimate the real erosion.

The remaining melting terms are small but have been included for completeness. They include an allowance for sensible heat transfer from the air when the air temperature, T_a, is greater than T_i, sublimation due to latent heat loss or gain to the air and a solar heating parameterized as a function of latitude and time of year. There can also be additions to the iceberg mass through solid precipitation if $T_a < 0$°C. All of the melting terms are distributed over the appropriate surface, whether aerial or under-water, and then the iceberg draught is adjusted to reflect the new mass.

3.3. Forcing fields and numerical procedure

Individual icebergs move through a simple discretisation of Eq. (2), as in Smith (1993), using timesteps of 135 s. Their melting, and the test for roll-over, are implemented at the end of each time step. If a berg collides with a coastline it is deemed to have become stranded and is no longer considered. This is not always realistic—some bergs can remain grounded at the coast for some time, for example in Hamilton Inlet, Labrador (Gustajtis and Buckley, 1978), and then move back off-shore. However, if a berg has moved into water shallower than its draught, but not actually collided with an ocean model coastline grid-box, then V_i is set to zero and the berg is allowed to melt each timestep until it is able to refloat. A number of locations, particularly off East Greenland and the Eurasian Arctic islands, have shelf waters sufficiently shallow that the larger bergs released from these sites because of the calving criterion (Table 3) must sit at their release points for some time before melting sufficiently that they can begin to move. Accounts of shallow fjord exits (Dowdeswell et al., 1992), stationary bergs around the larger glaciers of Svalbard (Dowdeswell, 1989) and Franz Josef Land (Dowdeswell et al., 1994), and ice plough marks in shallow seas (Solheim et al., 1988) are consistent with there being both initial and mid-journey iceberg grounding.

The dynamics and thermodynamics require a number of seasonally varying atmospheric and oceanic parameters. These are supplied from the climatology of an atmospheric general circulation model—the control run of Valdes and Hall (1994)—and an oceanic general circulation model driven, in robust diagnostic mode for 10 years, by the winds of the atmospheric model and the Levitus and Boyer (1994) climatology of ocean temperature and salinity. The ocean model covers the North Atlantic and Arctic Oceans at 1° horizontal resolution (Bigg et al., 1996; Wadley et al., 1996) and nineteen levels in the vertical, on a rotated latitude–longitude system (see Fig. 1). The model bathymetry, used to determine iceberg grounding, comes from the DBDB5 data set (US Naval Oceanographic Office, 1983). The open boundary in the South Atlantic, at approximately 23°S, uses the open boundary condition of Stevens (1991). Monthly sea-ice fields were digitised from the Bourke and Garrett (1987) climatology of Arctic sea-ice thicknesses. Some atmospheric and oceanic forcing fields for mid-July, namely T_s, V_w, and V_a, are shown in Fig. 1. These will be useful for later reference in Section 4.

The iceberg trajectory model was driven by linear interpolation of these various monthly average forc-

ing fields. While sub-surface information was available from the ocean model, only the surface fields were used in practice. For all except the deepest bergs this does not cause any significant error as the upper two or three levels in the ocean model tended to have similar properties over the regions in which icebergs are found.

A finer resolution ocean model of the Labrador Sea and North Atlantic, with 0.25° horizontal resolution but still nineteen levels in the vertical, was also developed in order to study the main iceberg routes down the Labrador and Greenland coasts in more detail (Section 4.6). This too used the robust diagnostic method, with barotropic flow on the open

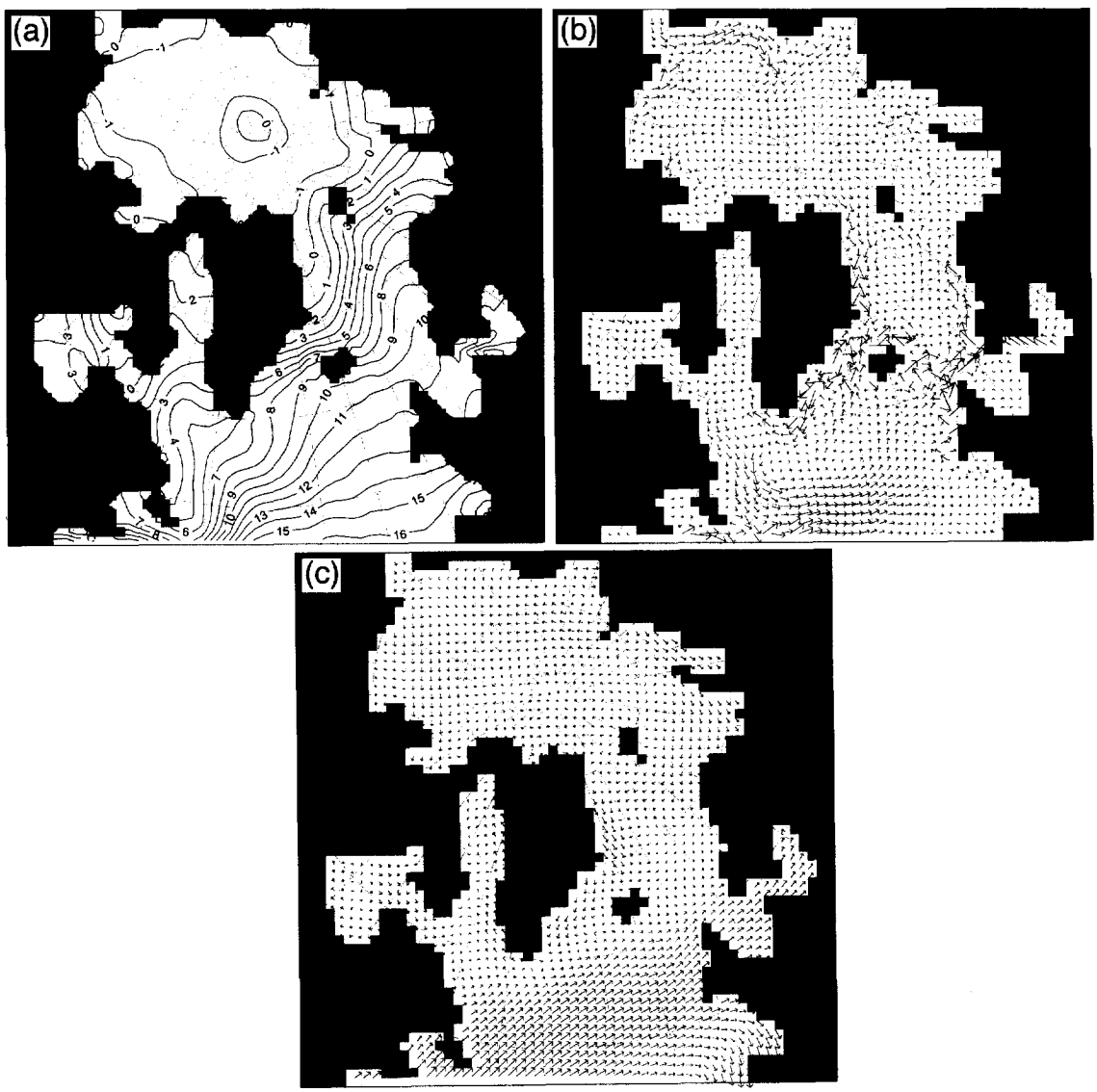

Fig. 1. Atmospheric and oceanic forcing fields from mid-July for the iceberg model: (a) sea surface temperature (in °C); (b) near surface currents (an arrow extending over 1 model grid point represents 0.05 m s^{-1}); (c) surface wind field (an arrow extending over 1 model grid point represents 4 m s^{-1}). Note that this view is a sub-section of the full ocean model, which actually extends to about 20°S.

boundaries determined by the outer coarse model and the baroclinic flow determined using the open boundary conditions of Stevens (1991). Only one model year was simulated with this fine model because of the inherent tendency for incompatibilities to develop at the open boundaries of such nested ocean models (Wadley and Bigg, 1996).

4. Results

4.1. Dominant forces and their geographical distribution

For the majority of trajectories, both in space and time, the dominant forces affecting the motion of the

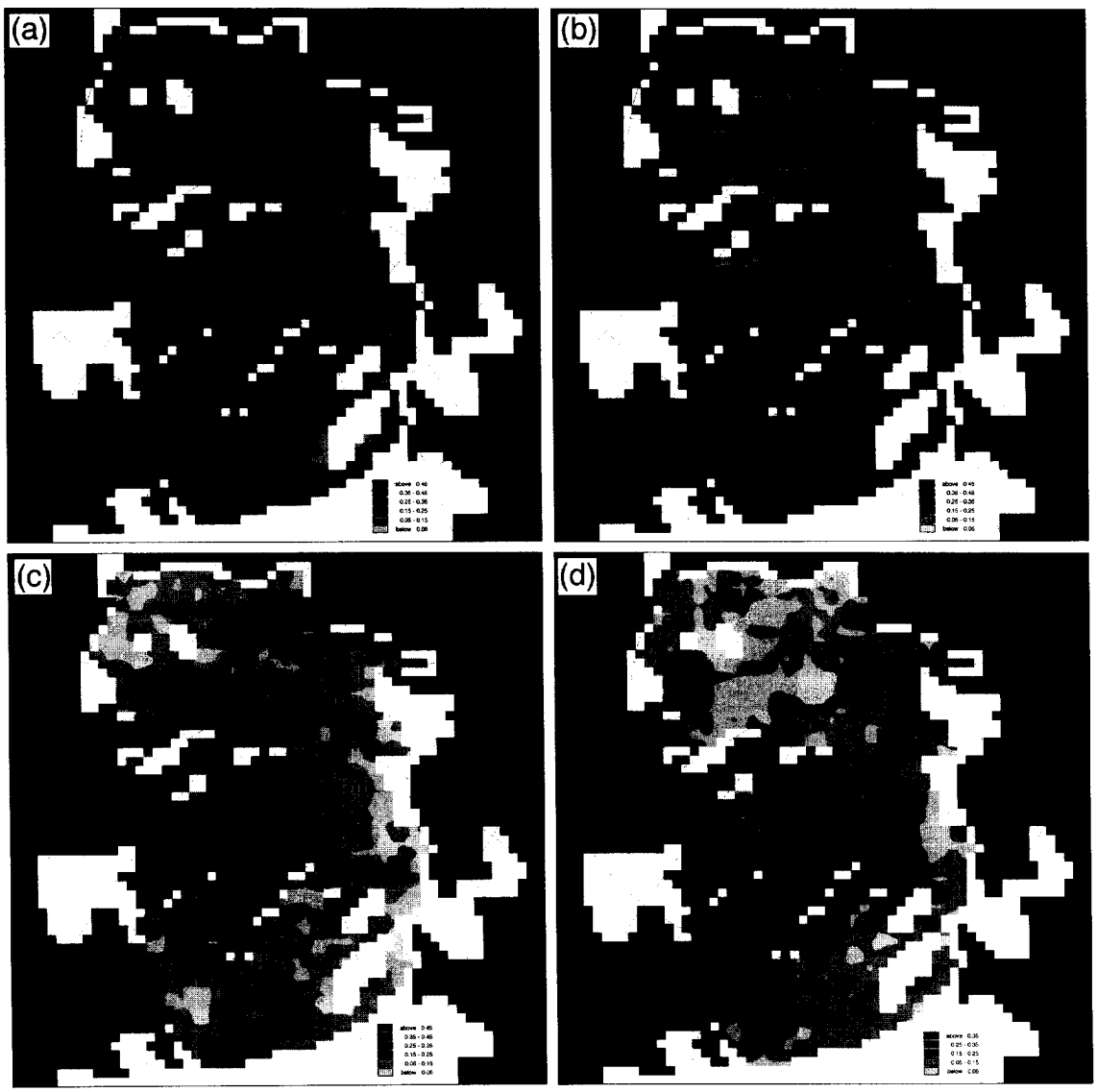

Fig. 2. The distribution of the mean contribution of the zonal component of different forces to iceberg motion as a proportion of the gross sum of all force components: (a) $M\mathrm{d}\boldsymbol{V}_w/\mathrm{d}t$; (b) $\boldsymbol{F}_w$; (c) $Mf\boldsymbol{k}\boldsymbol{x}(\boldsymbol{V}_i - \boldsymbol{V}_w)$; (d) $\boldsymbol{F}_a$; (e) $\boldsymbol{F}_r$. The contour interval is 10%.

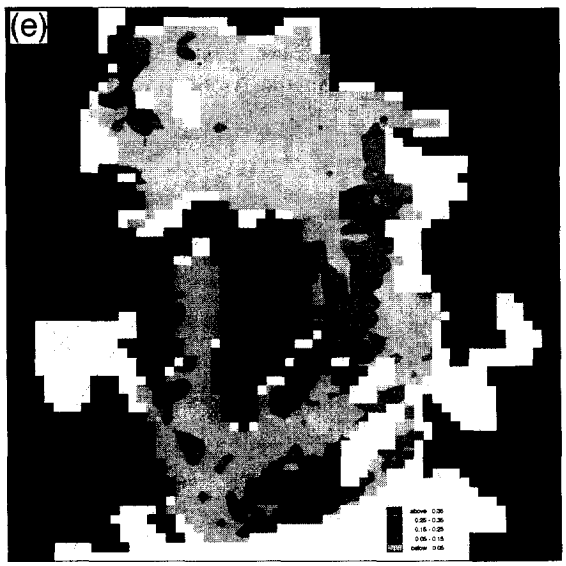

Fig. 2. (continued).

iceberg are the pressure gradient force, $\boldsymbol{F}_p$ and the water drag, $\boldsymbol{F}_w$ (Fig. 2). This is true regardless of the size of the berg. Within $\boldsymbol{F}_p/M$ (Eq. (6)) the key term is the material derivative, $d\boldsymbol{V}_w/dt$, not the geostrophic term. Bigg et al. (1996) showed that only with this term included could the most important iceberg zone east of Labrador and Newfoundland be reproduced. These two forces, $Md\boldsymbol{V}_w/dt$ and $\boldsymbol{F}_w$ (Fig. 2a, b), contribute approximately $70 \pm 15\%$ of the total forcing of iceberg motion, and tend to occur in a rough balance. Accelerations are generally smaller than 10^{-7} m s^{-2} (i.e. 1 cm s^{-1} day^{-1}), except immediately after grounded bergs have refloated. This rough balance demonstrates that icebergs are basically advected by the ocean current in which they are embedded, but subject to other forces sufficiently large that these produce enough off-set from pure advection in the iceberg's motion for water drag to be a significant retardant.

The Coriolis force and the air drag generally make up roughly equal amounts (15% each) of the remainder of the force balance (i.e. the terms producing the off-set from pure advection). It should be noted that the Coriolis force of Fig. 2c includes the geostrophic component of the pressure gradient term due to the term rearrangement that occurs when Eqs. (2) and (6) are combined. The ice drag is negligible in almost all circumstances, whilst the wave radiation force generally contributes less than 5% of the total force on a berg, but locally can be rather more significant (Fig. 2e).

There are key regions where the forcing regime diverges from the above pattern. In the Arctic, north of Greenland, the Coriolis force replaces the water drag as the force roughly balancing $Md\boldsymbol{V}_w/dt$, with the air drag also becoming more important to the west of this area, north of the Nares Strait between Ellesmere Island and Greenland. This re-ordering occurs because of a general weakening of the force components, as can be seen from the often erratic trajectories in this area (see Fig. 3, and Figs. 9 and 12 later). In contrast, another area shows increasing force magnitudes with a decline in the importance of the Coriolis term. This is in the East Greenland Current, and the Greenland Sea south of Svalbard. Both $\boldsymbol{F}_a$ and $\boldsymbol{F}_r$ become important second-order forces, because of the stronger local wind forcing (Fig. 1c). This is also true in the central North Atlantic south of Greenland, where a few bergs encounter the northern edge of the westerlies, and to the west of SW Greenland. The importance of the different melting terms is included as part of the discussion of iceberg life histories in Section 4.5.

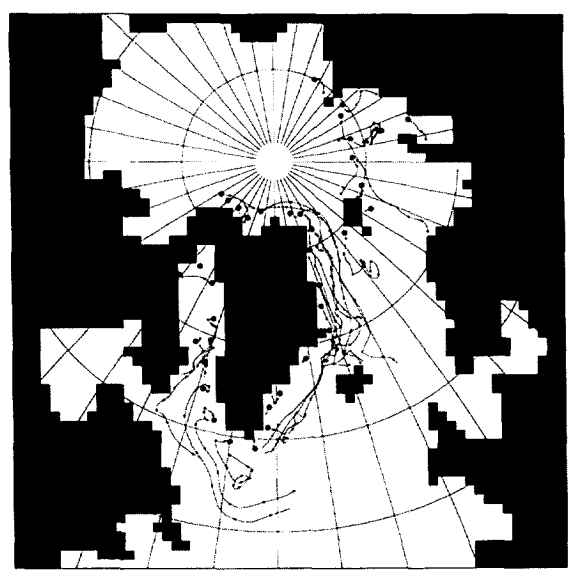

Fig. 3. Typical trajectories for icebergs of size 3 released on 1 October. The larger dots represent the sites of iceberg release and the small dots occur each 20 days along a trajectory.

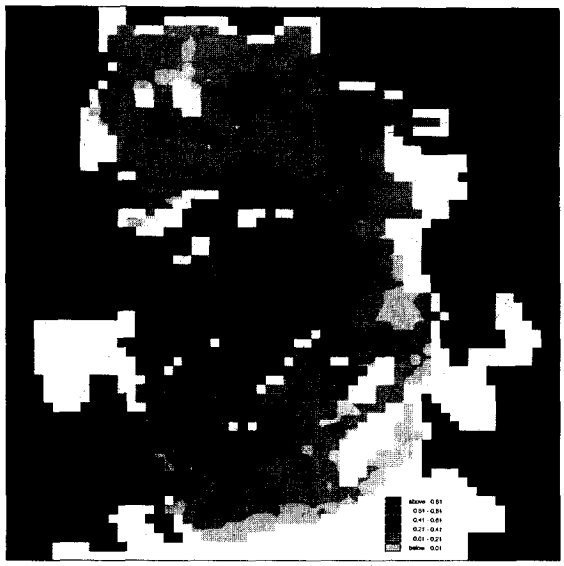

Fig. 4. Mean iceberg density in terms of the proportion of model dumps (which occur every 5 days) in which at least 1 berg is found in a given 110 km square. The contour interval is 20%. Regions where this approaches a value of 1 (oceanic blocks) are where icebergs are grounded or very slow moving.

4.2. Iceberg density

Bigg et al. (1996) showed that the iceberg limits of this model matched those observed relatively well. However, the model can also predict the iceberg density. Fig. 4 shows the average number of bergs in each 110-km-sided grid square at any one time that location data were stored (i.e. every 5 days), taking both the initial size distribution and the length of time over which the modelled icebergs survived into account. The size distribution was scaled so that there was one berg of class 10 for every three of class 1 (as per the fractional weighting column in Table 1), and so, for the purposes of this distributionally weighted diagram (Fig. 4), effectively 20 bergs in total were released per season from the sites with maximum calving flux (i.e., a size class 10 release site—see Table 3).

The limit of iceberg extent is shown well by the 1% contour, that is, where, using the above scaling, we expect to encounter a berg roughly once a year. However, the region enclosed by the 11% contour (i.e. roughly one berg every 50 days) is a much smaller subset of this larger area. Much of the Arctic Ocean, for example, may see an iceberg only occasionally, while still remaining within the iceberg limit. Nonetheless, there are clearly preferred paths from the release sites in the Arctic (Fig. 4, some of which can be seen in Fig. 3): from northern Green-

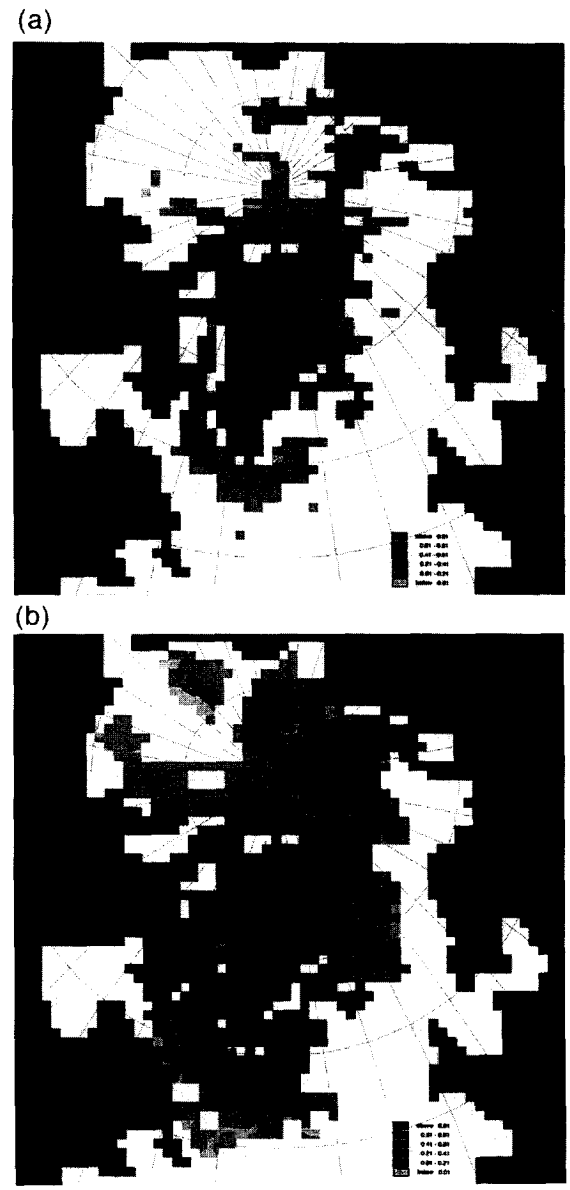

Fig. 5. Seasonal iceberg density, in terms of the proportion of model dumps (which occur every 5 days) in which at least 1 berg is found in a given 110 km square: (a) autumn; (b) winter. The contour interval is 20%. Regions where this approaches a value of 1 (oceanic blocks) are where icebergs are grounded or very slow moving.

land both westwards along the perimeter of the Canadian Arctic and eastwards into the East Greenland Current, westwards from the Russian Arctic into the East Greenland Current, and eastwards from Svernaya Zemlya towards the Siberian Arctic.

The main concentration regions outside of the Arctic occur because of either large numbers of sources (e.g. in Baffin Bay), or regions with strong currents into which the bergs have converged (e.g. the entire East Greenland Current or the East Icelandic Current north of Iceland), or a combination of these two influences (e.g. the Labrador Sea, where the East Greenland and Labrador Currents converge). Note that the localised spots of very high density occur because of shallow water, and consequent iceberg stranding. This is particularly noticeable in

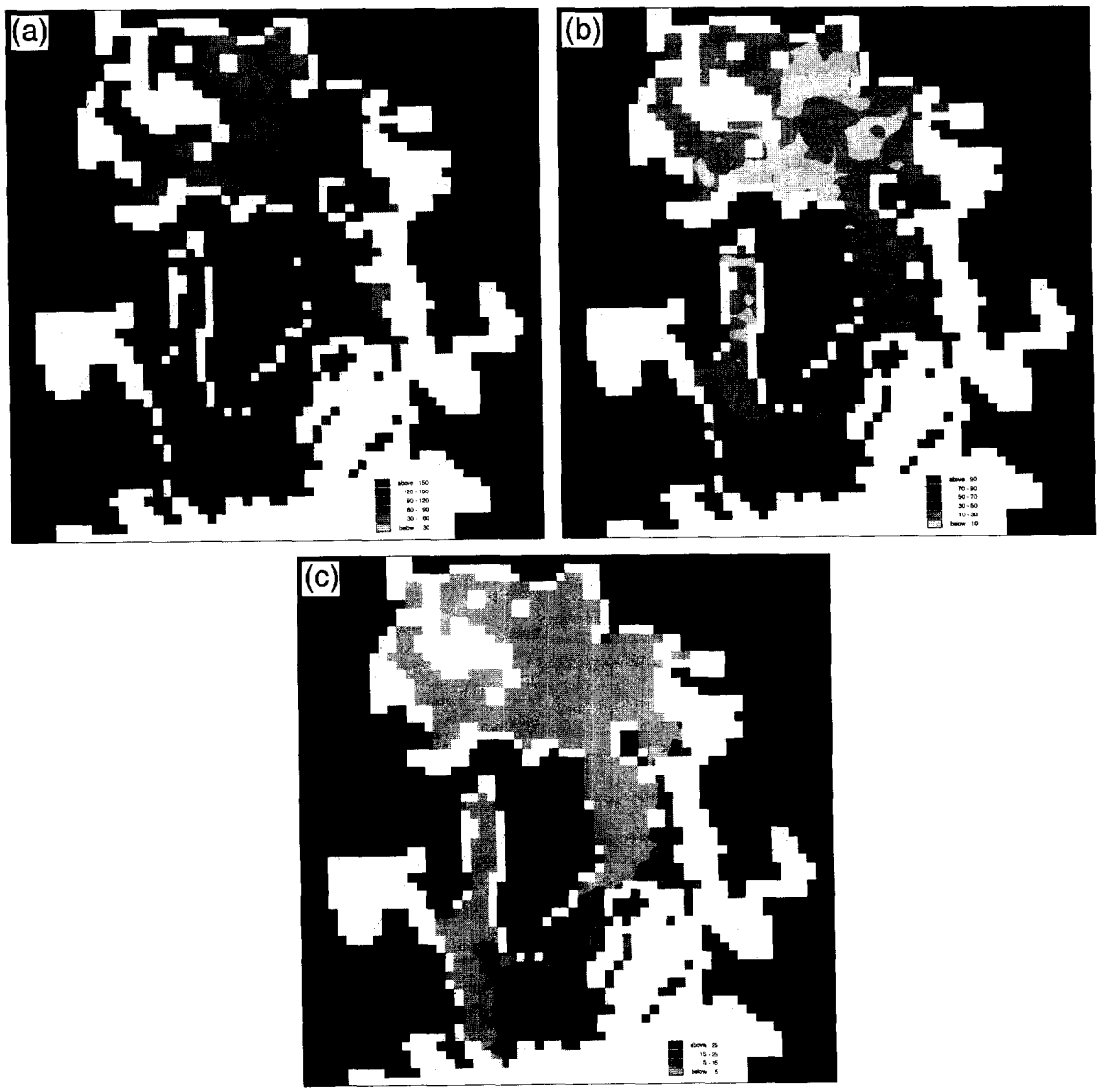

Fig. 6. Geographical distribution of the average melting rates of the three dominant melting terms: (a) wave breaking (aerially exposed vertical sides only); (b) turbulent heat transfer (bottom); (c) convection heat transfer (sub-surface vertical sides only). The contour interval is 30 cm day^{-1} for (a), 20 cm day^{-1} for (b), but 10 cm day^{-1} for (c).

the Russian Arctic near the point of calving origin, but also north of the East Siberian Islands where the shelf is very broad with depths less than 100 m to about 80°N.

The variation of the iceberg density field with season is striking. The most limited extent of the bergs is in autumn (September–November), when all major export routes have retracted to within 1000 km or so of the source glaciers (Fig. 5a). The most expansive field is in winter (December–February), when there is significant penetration towards 50°N in the Labrador Sea, into the North Atlantic southwest of Iceland, and into the Norwegian, Greenland and Barents Seas (Fig. 5b), as well as the central Arctic. The second most extensive season is spring (not shown), when significant numbers of bergs extend out to a few hundred kilometres poleward of the winter limits. Spring to early summer tends to be the time of maximum observed extent off Newfoundland (Marko et al., 1994); the modelled peak may be earlier due to the aseasonal modelling of iceberg release (see Section 4.4). The sudden increase in iceberg extent between autumn and winter, matching a real trend (Abramov, 1992, Marko et al., 1994), shows that climatological factors in ocean and atmospheric circulation play as important a role in iceberg trajectories as the seasonal variation in calving.

4.3. Size class effects

The initial size of the modelled iceberg is important in determining its trajectory for two major reasons: the variation in potential release sites with size class above 5 (Table 3) and the dependence of longevity on size. Thus bergs of classes 9 and 10 form a very small fraction of observed bergs in most

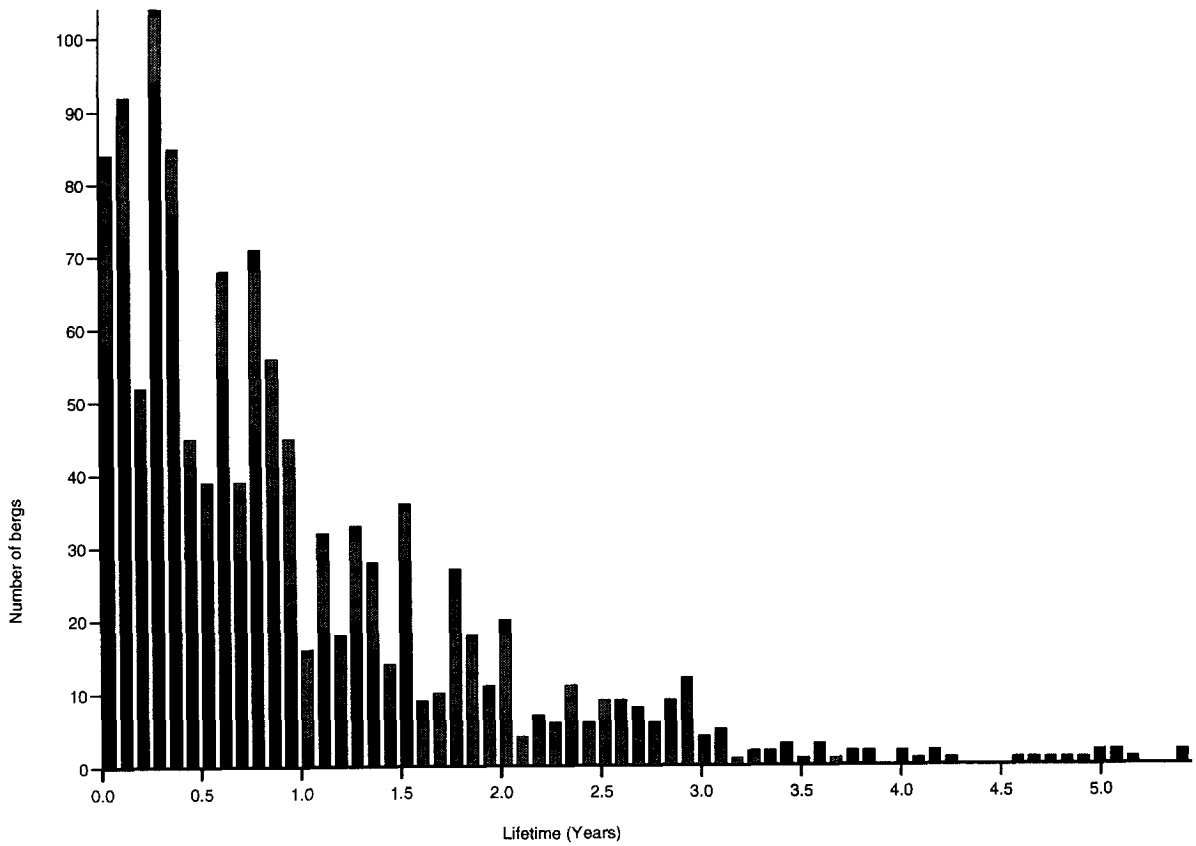

Fig. 7. Distribution of lifetimes of all bergs released, collected into monthly bins. The three sub-divisions per bar show, from bottom to top, the number of bergs initially in class sizes 1–3, 4–7, and 8–10, respectively.

regions, except for a zone in the Siberian Arctic, from 82° to 87°N, where together they make up about a quarter of the bergs that penetrate into this region. No modelled trajectory for these large bergs penetrated into the North Atlantic because of their limited, and geographically isolated, release sites.

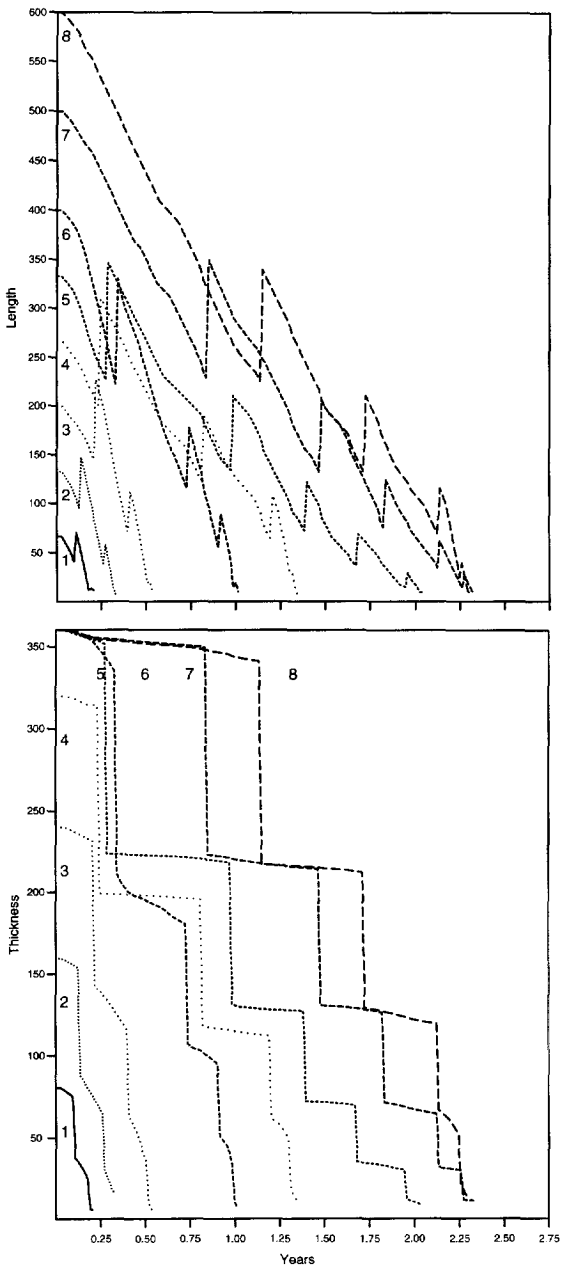

Fig. 8. Melting history of bergs from the 1 October release at 64°N, 57°W in southwest Greenland: (a) length (in metres); (b) total depth (in metres). The size class of the berg is noted at the beginning of the release. Overturning occurs at discontinuities in the curves.

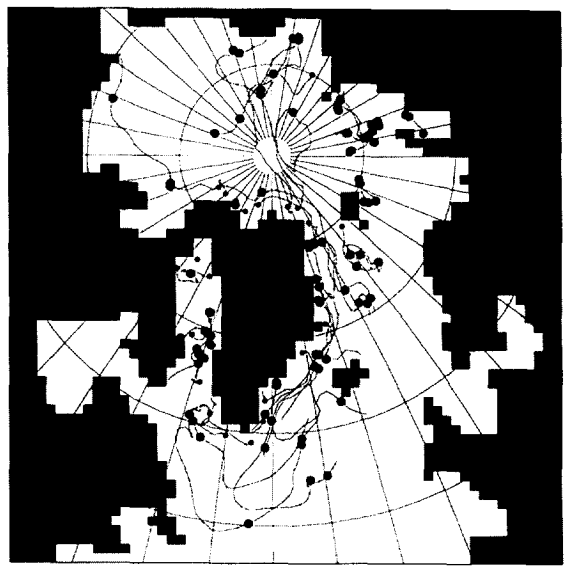

Fig. 9. Typical trajectories for icebergs of size 5 released on 1 October. The very largest dots show the locations of overturning, the mid-size dots represent the sites of iceberg release and the small dots occur each 20 days along a trajectory.

The smallest bergs, in contrast, form significant proportions (usually a majority) of those bergs in the most frequently occupied sectors of Fig. 4. For example, releases of such bergs from northern Greenland were able to circulate around a substantial part of the Beaufort Sea in the Canadian Arctic. While small bergs tend to melt before penetrating far into warmer seas, even bergs of class 2 were occasionally able to penetrate to 50°N in the Labrador Sea, even though the majority of bergs that were found south of 48°N originated as bergs of classes 5–8.

4.4. The role of seasonal releases

In our model the same number of bergs were released in each season. However, in reality, glacial calving will tend to peak during the summer (Dowdeswell, 1989) and autumn (Warren, 1992). The spatial density of icebergs was therefore examined for each seasonal release. In general, the patterns are similar, but with a few minor differences. Autumn releases have a lower probability of entering

the southern half of the Denmark Strait, between Iceland and Greenland, while summer releases are less likely to move southwest of Iceland. In contrast, those bergs entering the East Icelandic Current and moving northeast of Iceland tend to come from autumn and winter releases.

Two other minor differences may also be significant. Spring releases from northern Greenland form a majority of the bergs that circulate westwards into the Beaufort Sea. Further south, central Baffin Bay has a surprising minimum in iceberg density (Fig. 4). This occurs principally because only winter releases show a high probability of bergs entering this area. However, as our ocean model does not resolve the major searoutes through the Canadian Arctic—Lancaster Sound and Nares Strait, both of which are known to contain icebergs—the circulation field in the northern half of Baffin Bay may not be very accurate.

4.5. Iceberg lifetimes

The lifetimes of icebergs in the model varies from a few days to over 5 years. Those that survive only a few days invariably collide with the coastline within a few kilometres of their release site. It is common for several size classes of bergs from the same release point to suffer this fate because of the local forcing. Approximately a third of bergs are lost from the model from collision with the coast at some time in their history, with up to a tenth of these after crossing the entire Arctic Ocean. The only exception

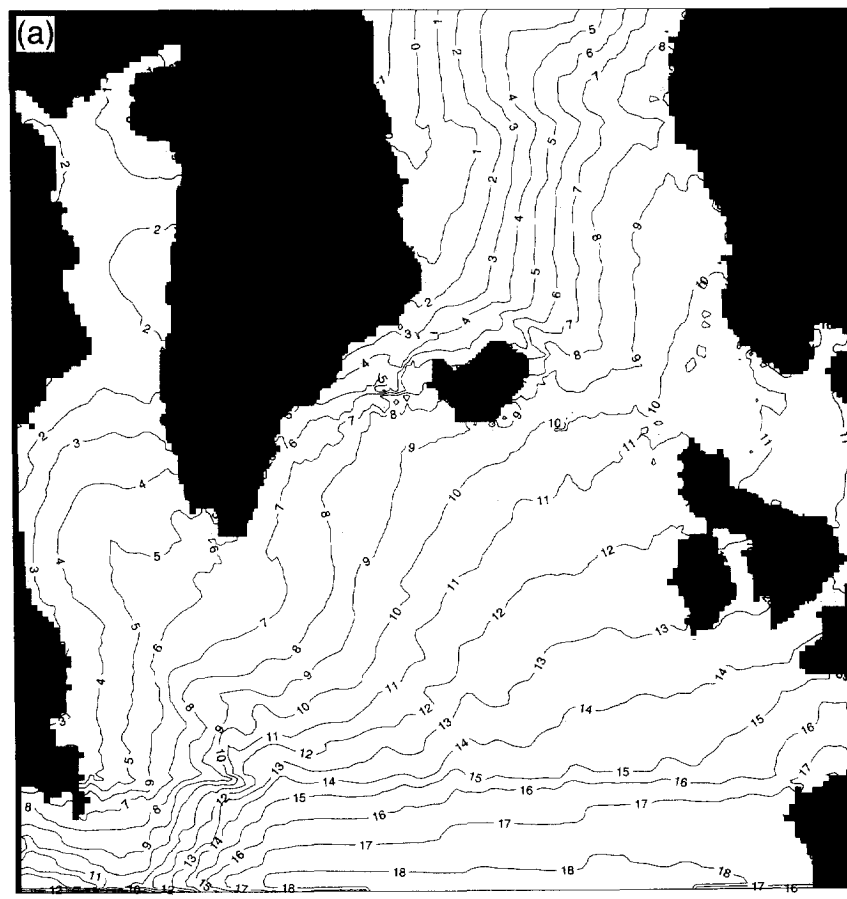

Fig. 10. Oceanic forcing fields from mid-July in the fine resolution ocean model: (a) sea surface temperature; (b) upper ocean current (an arrow extending over 1 model grid point represents 0.1 m s^{-1}).

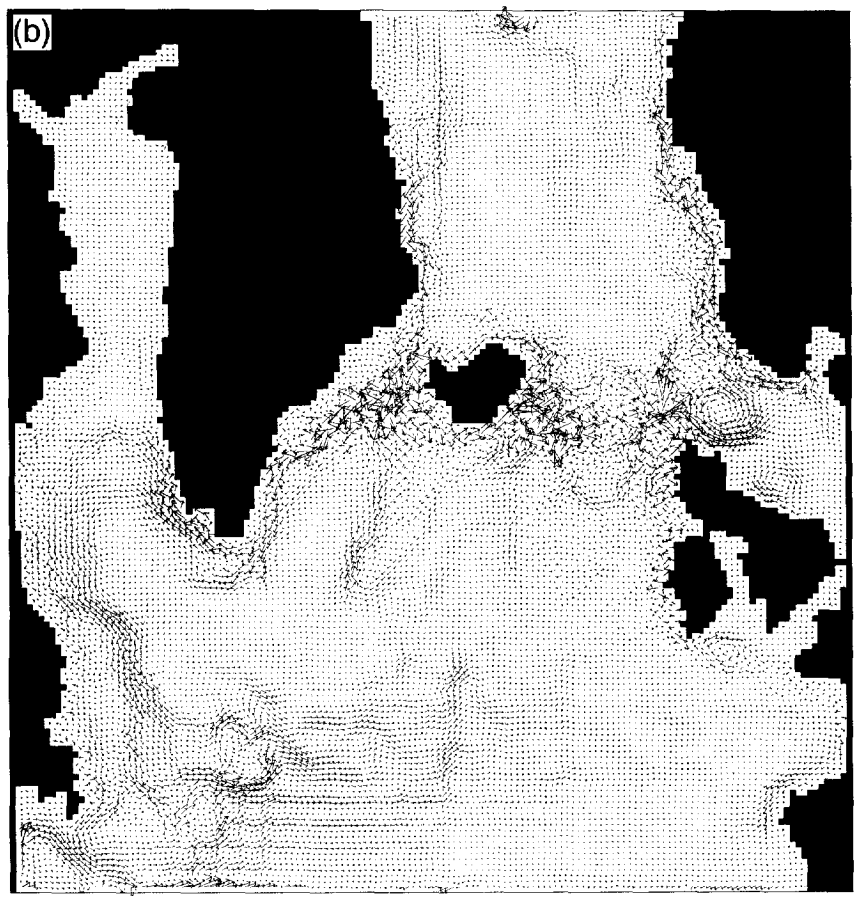

Fig. 10. (continued).

to this was with the spring release experiment, where only a quarter of bergs met this fate. Of the long-lived bergs only about 1% of each release of 285 bergs survives for more than 5 years. These are the largest bergs, that are released, and remain, in the Arctic, slowly decaying in the cold conditions.

The dominant melting term is the lateral erosion due to wave breaking (Eq. (10)). This can amount to more than 1 m day^{-1} (Fig. 6a) in regions of strong winds. Turbulent heat transfer (Eq. (8)) can be comparable in seas with temperatures above freezing (Fig. 6b), while melting due to convective heat transfer (Eq. (9)) is negligible until water temperatures are several degrees above 0°C, although it may then amount to more than 0.2 m day^{-1} (Fig. 6c). These three major terms all tend to reinforce each other in the zone of atmospheric westerlies near the oceanic temperature front of the North Atlantic Drift. The size of the terms here, combined with this reinforcement, means that the ultimate length of the trajectories of icebergs that reach the North Atlantic Drift will be quite sensitive to the details of the melting parameterisation, particularly the ad-hoc nature of wave erosion given by Eq. (10).

All other melting terms are never more than 0.01 m day^{-1}, and usually much less. It is of interest that the sublimation terms generally add volume to the bergs because of the lower saturation vapour pressure over ice than water and the coldness of the iceberg's surface compared to the surrounding water. The regions in which icebergs spend most of their lives also have sub-zero aerial temperatures, which

means that small mass additions due to snowfall are common.

The over-all distribution of lifetimes is roughly exponential (Fig. 7), but with a distinct plateau before 1 year. This discontinuity is caused by the predominance of class sizes 1–3 (50% of the total bergs); more than 80% of these bergs are lost in the first year, including all class 1 bergs. Class sizes 4–7, by contrast, are depleted by similar numbers each month over the first three years, although the variance can be large. Showing different behaviour again are the large bergs of class sizes 8–10, which show a distinct persistence: few are lost in the first year and most survive for at least 2.5 years.

Roughly half of the model berg observations are of bergs that have melted to size class 1 or smaller, even though only 15% of the total begin with this size. Only within a few hundred kilometres of the north, west and northeast Greenland coasts are size class 2 bergs more likely to be encountered. A typical melting history of bergs released from a southwest Greenland site is shown in Fig. 8. The

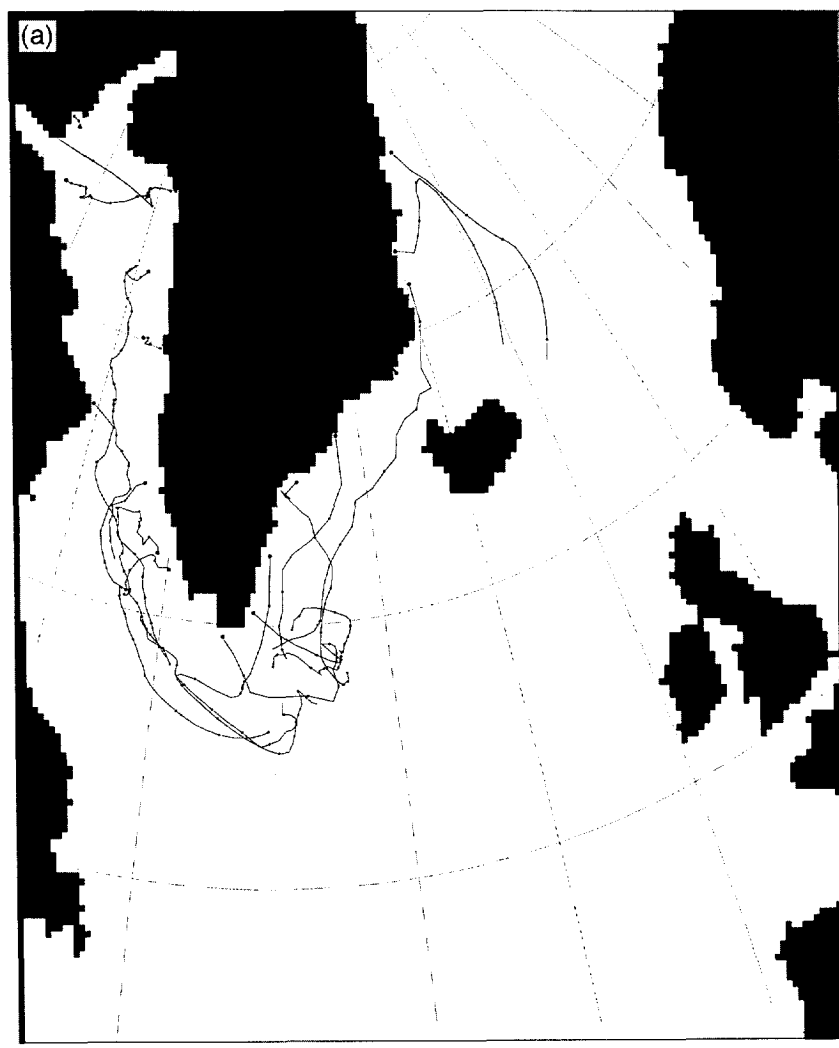

Fig. 11. Fine resolution iceberg trajectories corresponding to the 1 October releases of: (a) size class 3 (cf. Fig. 3); (b) size class 5 (cf. Fig. 9). The larger dots represent the sites of iceberg release and the small dots occur each 20 days along a trajectory.

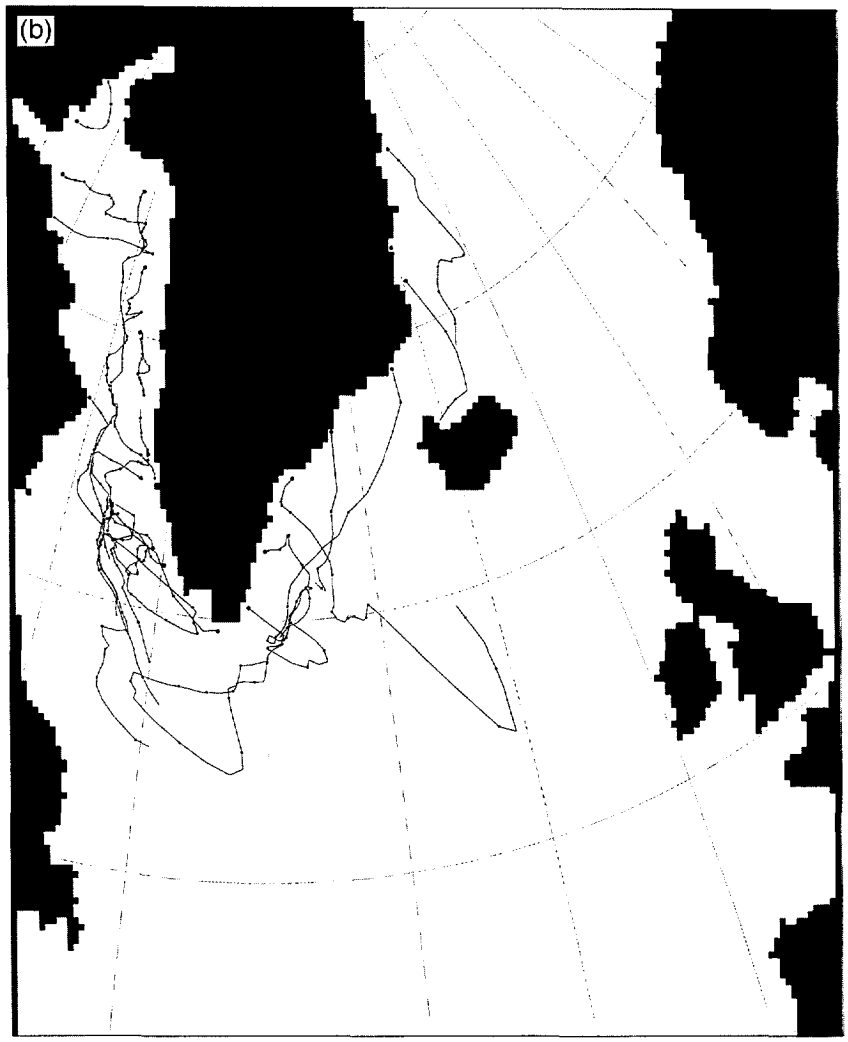

Fig. 11. (continued).

ablation processes act at a much faster rate on the horizontal dimensions of the bergs, except, in some instances, when the bergs become only a few tens of metres in length. This is mainly due to the wave friction term (Eq. (10), see also Fig. 6).

Fig. 8 also illustrates the effect of iceberg overturning, which is parameterised in the model. As the sides typically erode faster than the base or top many bergs thin to the point where their centre of gravity is too high and they pass the criterion for meta-stability (Eq. (7)). These points show up as discontinuities in length and depth, where after roll-over the new berg is longer, but shallower, than before. In reality the overturned berg should be wider, rather than longer, but the model always assume the berg has a given orientation to the water (Section 3.1). This will not significantly affect the conclusions, as discussed in Section 5.

The tendency for all bergs from a given source to roll-over once they have achieved similar dimensions is widespread. The length–depth combination at which this happens depends on the regional atmospheric, oceanic, and particularly wave climate. The independence of the erosion due to this latter feature from the dimensions of the berg (Eq. (10)) means that the smaller bergs will overturn sooner, as sug-

gested by Fig. 8. The larger bergs, having a fixed initial depth (Table 1), will all tend to roll-over around the same time after release. Note that there is a tendency for bergs to roll-over more frequently as they get smaller. Not all bergs will roll-over during their history, however, because of the dependence of the ablation mechanisms on regional climate.

In Fig. 9 the overturning locations are shown for a particular release of size class 5. Some bergs from northern Greenland and the Canadian Arctic do not overturn at all, or only very late in their life, as both atmospheric and oceanic conditions are of low thermal and kinetic energy. Those near the Davis Strait overturn a number of times, as do those in the Russian Arctic. There are also some incidences of double overturning, where one berg rolls twice within a short distance. A few instances, particularly for small bergs, of double roll-over within a season are seen in Fig. 8.

4.6. Sensitivity of trajectories to varied forcing

To examine the sensitivity of modelled iceberg trajectories to the imposed current field a finer resolution ocean model was run for the northern Atlantic (Section 3.3). Comparing the surface velocity and temperature fields of this model (Fig. 10) with those of the coarser model (Fig. 1) shows that such important features as the Labrador Current and the East Greenland Current are better resolved in the finer model. It needs to be noted, however, that in the finer model, Hudson's Bay was closed off from the Labrador Sea for numerical reasons. This could have a distorting effect on the flow field in this region.

As typical examples, the fine resolution model's trajectories for the two examples seen so far (Figs. 3 and 9) are given in Fig. 11. Comparison of these diagrams shows similar features in the trajectory fields and principal paths, but significant differences in detail. Fine and coarse model trajectories both show similar entrainment in the East Greenland Current and similar looping of trajectories about the southern tip of Greenland, Cape Farewell. Both show regions of convergence and stagnation off the southwest and southeast coasts of Greenland (near (62°N, 55°W and 60°N, 37°W, respectively). In both models bergs released from the very north of Baffin Bay tend to remain north of the Davis Strait.

A very noticeable difference, however, is that the coarse resolution model is more easily able to transport bergs into the Labrador Current, and thus has a much greater probability of bergs reaching the Grand Banks. This behaviour is more realistic than that in the fine model so the stagnation region in the centre of the Labrador Sea must be too intense in the finer model. The absence of the Hudson Bay connection may be responsible for this, as it removes one of the pathways for water turning west after rounding Cape Farewell in the East Greenland Current.

There are two differences which may show greater reality in the fine resolution model. One is the lesser tendency for bergs to be entrained in the East Icelandic Current (note the cyclonic gyre structure in Fig. 10b to the northwest of Iceland, and the narrowness of the coastal current, which contrasts with the wider eastwards current of Fig. 1b). The other is the greater ability of bergs from the southern half of Baffin Bay to penetrate Davis Strait in the stronger southward current (see Fig. 10b) along Baffin Island, and travel south of 60°N.

An alternative way to test the sensitivity of the modelled trajectories is to use slightly different starting dates. The bergs will then be subject to small differences in the forcing fields. The trajectories of three mid-winter releases separated by 3 days each are shown for size class 5 in Fig. 12. These show very clearly how sensitive the iceberg trajectories are to the actual forcing. In some areas, such as the Siberian Arctic, the atmospheric and oceanic climatological seasonal cycle is very small and there are thus only minor differences between the three realisations. However, in other areas the amplitude of the seasonal cycle is very much greater and while the general picture of iceberg tracks east and southwest of Greenland, for example, is uniform, the detailed response of the icebergs produces very different trajectories. In other regions, such as north of Greenland and Ellesmere Island, radically different paths are possible despite the small variation in seasonal climatology. Here, the trajectories exhibit distinctly chaotic behaviour, with small differences in position resulting in iceberg entrainment in very different current systems.

Another test of the sensitivity of the model involves variation in the roll-over criterion. Simulations were carried out with several less stringent

roll-over conditions, so that roll-over would occur less frequently. The resulting trajectories all had the same general characteristics we have seen earlier in this section—namely, reproduction of the pattern but considerable divergence over the detail of the trajectories. In addition, however, allowing thinner, higher bergs tended to reduce the numerical stability of Eq. (2). The timestep had to be shortened in proportion to the degree of thinness of the berg.

5. Discussion

The sensitivity of the details of modelled iceberg trajectories to the driving (and melting) mechanisms

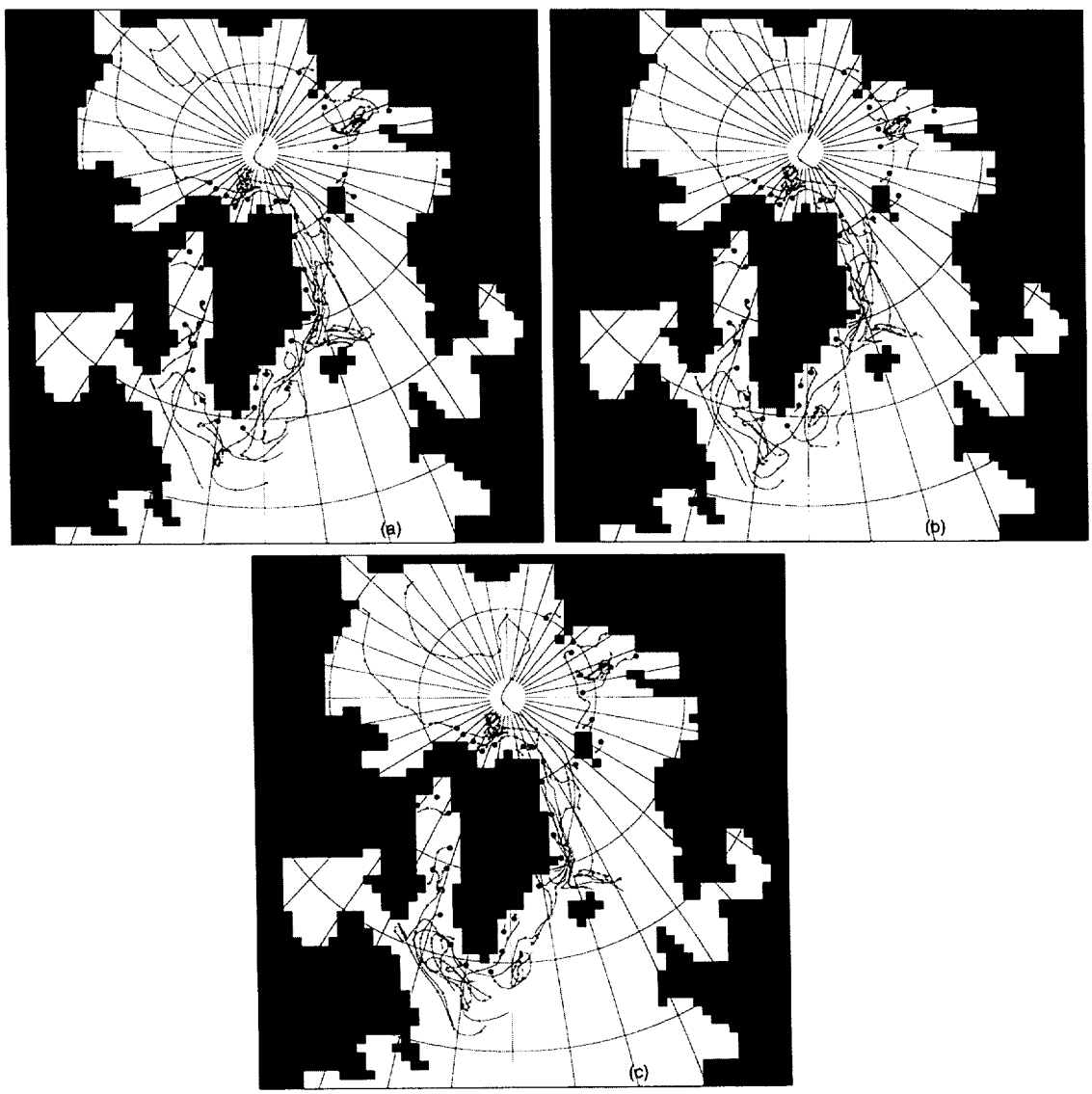

Fig. 12. Trajectories from three releases of size 5 bergs over a week: (a) release on 28 December; (b) release on 1 January; (c) release on 4 January. The larger dots represent the sites of iceberg release and the small dots occur each 20 days along a trajectory.

shown in Section 4.6 means that reproduction of any real, individual, iceberg track would be extremely unlikely. The oceanic and atmospheric conditions experienced by the berg each day will determine its actual path, not the climatological fields used in this model. However, the general zones of movement and melting reproduced by the model are retained in the sensitivity experiments enabling us to compare the general findings of the model with the rather limited observational evidence.

Bigg et al. (1996) showed that this model reproduces the observed southward iceberg limit in the North Atlantic reasonably well. Comparison of the modelled density is more difficult as there are few observations. The Labrador Sea and Davis Strait are well monitored by the International Ice Patrol, but information is often presented in terms of overall indices (e.g. the Davis Strait Ice Index, or the number of bergs south of a given latitude, Marko et al. (1994)). Comparison of Ice Patrol charts (Newell, 1993), or tracked bergs (Dempster and Bruneau, 1975; Gustajtis and Buckley, 1978; Robe et al., 1980; Marko et al., 1982; Venkatesh et al., 1994) show similar paths and behaviour of individual bergs. The tendency for occasional localised rotations occurs in both model and data, particularly in the model, in certain regions where the prevailing currents are weak. The model tends not to allow bergs to penetrate as close to the Labrador/Newfoundland coast as observations suggest can happen, although a few tracks in the coarse resolution ocean model simulations (not illustrated) hug the coast. The distribution of bergs in the Barents Sea (Abramov, 1992) shows clustering southwest of Svalbard extending towards the North Cape, and many bergs close to Franz Josef Land (Sater et al., 1971; Dowdeswell et al., 1994); both features are seen in Fig. 4. Pavlov and Pfirman (1995) note icebergs in the Kara Sea (c. 72°N, 75°E) where Fig. 4 shows a distinct maximum in iceberg density.

The detailed path of bergs from West Greenland in the Labrador Sea and Baffin Bay was thought by Marko et al. (1982) to be in an anticlockwise gyre around Baffin Bay before issuing into the Labrador Sea, while Gustajtis and Buckley (1978) thought southern Greenland bergs circumvented Baffin Bay by crossing Davis Strait. Marko et al. (1994) show both paths. The modelled trajectories predominantly follow the southern path, crossing the Davis Strait, or the northern part of the Labrador Sea (Figs. 3 and 9). West Greenland bergs released within Baffin Bay rarely move anticlockwise, but drift out into Baffin Bay before being entrained in the southward-flowing boundary current along Baffin Island. Bergs released at the northern end of Baffin Bay almost invariably remain in this region. The ocean model providing the driving current field is unable to resolve Lancaster Sound or Nares Strait, which may mean that modelled currents are weaker than reality in this region.

Observations of bergs in the Arctic are limited but generally consistent with the main pathways of the modelled bergs (Herman et al., 1989). Some bergs track almost directly over the North Pole from Greenland to eastern Siberia (Fig. 5a and Fig. 9). This is not due to advection in the ocean current, as the ocean model's surface layer flow (Fig. 1b) agrees with the generally southward flow into the East Greenland Current seen in sea-ice drift (Schlosser et al., 1995). Note from Fig. 2 that this is a region where air drag is more significant and directed towards Eurasia (Fig. 1c), so if a berg moves towards the North Pole, where currents are weaker, it can drift slowly towards Siberia. Herman et al. (1989) noted some bergs with this behaviour.

There is some limited information on iceberg masses in the Labrador Sea, from measurements on beached bergs (Marko, 1982; Marko et al., 1994). This suggests that about 50% of bergs in this area should have melted to class size 1 or smaller, 45% to between size 1 and 2, and only 5% remain greater than size class 2. The modelled bergs are released with rather more bigger bergs (see Table 1), but 30–50% of these bergs in the Labrador Sea have melted to be smaller than size class 1 by the time they reach the Labrador Sea (Fig. 13) and 60–90% are smaller than size class 2, with more smaller bergs occurring near the Labrador coast. The release distribution of modelled bergs, and the melting parameterisation, is therefore consistent with observations.

Estimates of the lifetimes of bergs of varying sizes have been made by Venkatesh and El-Tahan (1988) for the Labrador Sea. Extrapolating from their data suggests that our size class 1 bergs should survive of the order of 100 days, size class 2 bergs up to a year and bigger bergs for possibly several years. This is roughly consistent with Fig. 7. About

Fig. 13. Proportion of icebergs in each 110-km square that have melted to, or below, the mass of size class 1. The contour interval is 20%.

20% of modelled bergs have lifetimes of the order of three months (15% were of size class 1, Table 1) and another 30% last up to a year (15% were of size class 2). Given that our modelled lifetimes include losses due to beaching, and so Fig. 7 will be biased towards shorter lifetimes than bergs that remain at sea, our lifetime estimates are compatible with those for Venkatesh and El-Tahan (1988).

It is, finally, worth commenting on the validity of the wave erosion Eq. (10). The relative success of the model in reproducing the generalities of iceberg motion, as shown above, suggests that Eq. (10) is not totally unreasonable as a simulation of wave erosion. This is reinforced by the consideration that this term is the strongest melting term by far, being especially large in the stormy zones of fastest melting in the northern Atlantic, but where the model still gives sensible trajectories.

6. Conclusions

The mean properties of the iceberg trajectory model described here have been shown to be generally consistent with climatological observations, although the model has not been tested on any one individual berg's history. Our knowledge of iceberg distributions and dynamics, however, is still limited as tracking individual bergs routinely, using satellite imagery for instance, is in its infancy (Willis et al., 1996). Therefore, assuming our model is at least moderately realistic, we may be able to use it to infer information about geophysical processes in regions that are currently difficult to access. One example where our model may be useful is in determining glacial calving rates. Detailed comparison of the modelled trajectories of individual tidewater glacier releases with present knowledge of iceberg limits, the distribution and geology of iceberg-carried lithogenic debris on the ocean floor and $\delta^{18}O$ measurements of individual icebergs at sea could help to determine the berg size range distribution and their seasonal flux for that release point. Knowledge of past iceberg limits, through analysis of sedimentary debris, may also be used to verify iceberg trajectories within a palaeoceanographic model of the North Atlantic.

Whether the Greenland and Antarctic ice sheets are ablating or growing is an important question in the current debate about climatic change and potential sea level rise. Better estimates of iceberg calving will help address this question. Another geophysical problem the iceberg model can help address is the nature and strength of the Arctic Ocean and Greenland Sea circulation. This is poorly known due to the difficulty of measuring current flow under sea-ice. Better knowledge of iceberg movement in these areas could be used to validate ocean models through the iceberg model intermediary. As iceberg studies have the potential to help address many other geophysical and climatic questions we hope that this model may foster their increase.

Acknowledgements

This work was supported by the NERC under grant GST/02/1179. We would like to thank Paul Valdes of Reading University for supplying the atmospheric model wind fields used to force our ocean models.

References

Abramov, V.A., 1992. Russian iceberg observations in the Barents Sea. Polar Res. 11, 93–97.

Andrews, J.T., Milliman, J.D., Jennings, A.E., Rynes, N., Dwyer, J., 1994. Sediment thicknesses and Holocene glacial marine sedimentation-rates in 3 East Greenland fjords (c. 68°N). J. Geol. 102, 669–683.

Bigg, G.R., Wadley, M.R., Stevens, D.P., Johnson, J.A., 1996. Prediction of iceberg trajectories in the North Atlantic and Arctic Oceans. Geophys. Res. Lett. 23, 3587–3590.

Bourke, R.H., Garrett, R.P., 1987. Sea ice thicknesses in the Arctic Ocean. Cold Reg. Sci. Technol. 13, 259–280.

Chirivella, J.E., Miller, C.G., 1978. Hydrodynamics of icebergs in transit. In: Husseiny, A.A. (Ed.), Proceedings of the First Conference on Iceberg Utilization for Freshwater Production. Iowa State University, pp. 315–333.

Dempster, R.T., Bruneau, A.D., 1975. Dangers presented by icebergs and protection against them. In: Malaurie, I.J. (Ed.), Arctic Oil and Gas: Problems and Possibilities. Moutan, Paris, pp. 348–362.

Dowdeswell, J.A., 1989. On the nature of Svalbard icebergs. J. Glaciol. 35, 224–234.

Dowdeswell, J.A., Whittington, R.J., Hodgkins, R., 1992. The sizes, frequencies, and freeboards of East Greenland icebergs observed using ship radar and sextant. J. Geophys. Res. 97 (C3), 3515–3528.

Dowdeswell, J.A., Gorman, M.R., Glazovsky, A.F., Macheret, Y.Y., 1994. Evidence for floating ice shelves in Franz-Josef-Land, Russian high Arctic. Arct. Alpine Res. 26, 86–92.

Eckart, E.R.G., Drake, R.M., 1959. Heat and Mass Transfer. McGraw-Hill, New York, 530 pp.

El-Tahan, M.S., Venkatesh, S., El-Tahan, H., 1987. Validation and quantitative assessment of the deterioration mechanisms of Arctic icebergs. J. Offshore Mech. Arct. Eng. 109, 102–108.

Garrett, C.J.R., 1985. Statistical prediction of iceberg trajectories. Cold Reg. Sci. Technol. 11, 255–266.

Gill, A.E., 1982. Atmosphere–Ocean Dynamics. Academic Press, New York, 662 pp.

Gustajtis, K.A., Buckley, T.J., 1978. A seasonal iceberg density distribution along the Labrador coast. In: Muggeridge, D.B. (Ed.), Fourth International Conference on Port and Ocean Engineering under Arctic Conditions. Memorial University of New Foundland, St. John's, New Foundland, pp. 972–983.

Harvey, J.G., 1976. Atmosphere and Ocean. Artemis Press, London, 143 pp.

Herman, Y., Osmond, J.K., Somayajulu, B.L.K., 1989. Late Neogene Arctic paleoceanography: micropaleontology, stable isotopes and chronology. In: Herman, Y. (Ed.), The Arctic Seas. Van Nostrand Reinhold, New York, pp. 581–655.

Higgins, A.K., 1990. North Greenland glacier velocities and calf ice production. Polarforschung 60, 1–23.

Isaacson, M., McTaggart, K.A., 1990. Modelling of iceberg drift motions near a large offshore structure. Cold Reg. Sci. Technol. 19, 47–58.

Koryakin, V.S., 1986. Decrease in glacier cover on the islands of the Eurasian Arctic during the 20th century. Polar Geogr. Geol. 10, 157–165.

Levitus, S., Boyer, T.P., 1994. World Ocean Atlas. CD-ROM, NOAA.

Løset, S., 1993. Thermal energy conservation in icebergs and tracking by temperature. J. Geophys. Res. 98 (C6), 10001–10012.

Marko, J.R., 1982. The Ice Environment of Eastern Lancaster Sound and Northern Baffin Bay. Indian and Northern Affairs Canada Environmental Studies No. 26, 203 pp.

Marko, J.R., Birch, J.R., Wilson, M.A., 1982. A study of long-term satellite-tracked iceberg drifts in Baffin Bay and Davis Strait. Arctic 35, 234–240.

Marko, J.R., Fissel, D.B., Wadhams, P., Kelly, P.M., Brown, R.D., 1994. Iceberg severity off eastern North America: its relationship to sea ice variability and climate change. J. Climatol. 7, 1335–1351.

Meteorological Office, 1969. Marine Observer's Handbook, 9th ed. HMSO, London, 153 pp.

Morgan, V.I., Budd, W.F., 1978. The distribution, movement and melt rates of Antarctic icebergs. In: Husseiny, A.A. (Ed.), Proceedings of the First Conference on Iceberg Utilization for Freshwater Production. Iowa State University, pp. 220–228.

Newell, J.P., 1993. Exceptionally large icebergs and ice islands in eastern Canadian waters—a review of sightings from 1900 to present. Arctic 46, 205–211.

Orheim, O., 1987. Icebergs in the Southern Ocean. Ann. Glaciol. 9, 241–242.

Pavlov, V.K., Pfirman, S.L., 1995. Hydrographic structure and variability of the Kara Sea—implications for pollutant distribution. Deep-Sea Res. Part II 42, 1369–1390.

Pelto, M.S., Warren, C.R., 1991. Relationship between tidewater glacier calving velocity and water depth at the calving front. Ann. Glaciol. 15, 115–118.

Robe, R.Q., Maier, D.C., Russell, W.E., 1980. Longterm drift of icebergs in Baffin Bay and the Labrador Sea. Cold Reg. Sci. Technol. 1, 183–193.

Sater, J.E., Ronhovde, A.G., Van Allen, L.C., 1971. Arctic environment and resources. Arctic Institute of North America, Washington, 309 pp.

Schlosser, P., Swift, J.H., Lewis, D., Pfirman, S.L., 1995. The role of the large-scale Arctic Ocean in the transport of contaminants. Deep-Sea Res. Part II 42, 1341–1367.

Smith, S.D., 1993. Hindcasting iceberg drift using current profiles and winds. Cold Reg. Sci. Technol. 22, 33–45.

Smith, S.D., Banke, E.G., 1983. The influence of winds, currents and towing force on the drift of icebergs. Cold Reg. Sci. Technol. 6, 241–245.

Smith, S.D., Donaldson, N.R., 1987. Dynamic modelling of iceberg drift using current profiles. Canadian Techical Report of Hydrography and Ocean Sciences, No. 91, Dartmouth, pp. 125.

Solheim, A., Milliman, J.D., Elverhoi, A., 1988. Sediment distribution and sea-floor morphology of Storbanken: implications for glacial history of the northern Barents Sea. Can. J. Earth Sci. 25, 547–556.

Stevens, D.P., 1991. The open boundary condition in the United Kingdom Fine Resolution Antarctic Model. J. Phys. Oceanogr. 21, 1494–1499.

Strübing, K., 1974. Eisberge im Nordatlantik—60 Jahre International Ice Patrol. Wetterlotse 26, 141–160.

U.S. Naval Oceanographic Office and the U.S. Naval Ocean Research and Development Activity, 1983. DBDB5 (Digital Bathymetric Data Base—5 minute grid). USNOO, Bay St. Louis, Mississippi.

Valdes, P.J., Hall, N.M.J., 1994. Mid-latitude depressions during the last ice age. In: Duplessey, J.C. (Ed.), Long Term Climate Variations—Data and Modelling. Springer-Verlag, Berlin, pp. 511–531.

Venkatesh, S., El-Tahan, M., 1988. Iceberg life expectancies in the Grand Banks and Labrador Sea. Cold Reg. Sci. Technol. 15, 1–11.

Wadley, M.R., Bigg, G.R., 1996. The stability of passively nested ocean general-circulation models. Geophys. Astrophys. Fluid Dyn. 82, 207–219.

Wadley, M.R., Bigg, G.R., Stevens, D.P., Johnson, J.A., 1996. On the use of basin-scale ocean general circulation models faced by prescribed atmospheres in ocean climate studies. J. Phys. Oceanogr. (submitted).

Warren, C.R., 1992. Iceberg calving and the glacioclimatic record. Prog. Phys. Geogr. 16, 253–282.

Weeks, W.F., Campbell, W.J., 1973. Icebergs as a fresh-water source: an appraisal. J. Glaciol. 12, 207–233.

Weeks, W.F., Mellor, M., 1978. Some elements of iceberg technology. In: Husseiny, A.A. (ed.), Proceedings of the First Conference on Iceberg Utilization for Freshwater Production. Iowa State University, pp. 45–98.

Willis, C.J., Macklin, J.T., Partington, K.C., Teleki, K.A., Rees, W.G., Williams, R.G., 1996. Iceberg detection using ERS-1 synthetic-aperture radar. Int. J. Remote Sensing 17, 1777–1795.

Venkatesh, S., Murphy, D.L., Wright, G.F., 1994. On the deterioration of icebergs in the Marginal Ice Zone. Atmosphere Ocean 32, 469–484.